

A Possible Aeronomy of Extrasolar Terrestrial Planets

W. A. Traub and K. W. Jucks

Harvard-Smithsonian Center for Astrophysics, Cambridge, Massachusetts

Abstract.

Terrestrial planetary systems may exist around nearby stars as the Earth-sized counterparts to the many giant planets already discovered within the solar neighborhood. In this chapter we first discuss the numerous techniques which have been suggested to search for extrasolar terrestrial planets. We then focus on the expected results from that technique in which an orbiting telescope or interferometer is used to obtain a visible or infrared spectrum of a planet, without contamination from the parent star. We show examples of such spectra for selected cases: the present Earth, the Neoproterozoic (snowball) Earth, a methane-rich Earth, and the present Mars and Venus. We conclude by discussing the implications of such spectra for the detection of life on an extrasolar terrestrial planet.

To appear in "Atmospheres in the Solar System: Comparative Aeronomy", edited by M. Mendilo, A. Nagy, and H.J. Waite, AGU Geophysical Monograph 130, 369-380, 2002.

1. KNOWN EXTRASOLAR SYSTEMS

The first planet orbiting a solar-type star beyond the solar system was announced in 1995. Since then, as of October 2001, 66 planets have been found and confirmed, orbiting 58 stars with a median distance from the sun of about 28 pc. The search database contains roughly 1200 stars.

Current estimates of the frequency of massive planets range from about 3-5% to 6-7% [*J. Schneider, and G. Marcy, resp., personal communication*]. The number of detected planets is growing monthly, as observing techniques are refined, and as the time base of the record increases, allowing longer-period planet signatures to be extracted from the radial velocity sequences.

The definition of a planet can be a controversial issue, as is evidenced by the recent debate on whether Pluto should be classified as a planet, or a trans-Neptunian or Kuiper-belt object. However in the case of extrasolar planets the debate centers not on the question of the low-mass end of the scale, as for Pluto, but on the high-mass end, which is the realm of the planets discovered to date. The question is, should

these objects be classified as planets, brown dwarfs, or small stars?

Here we adopt the recommendation of *Oppenheimer et al.* [2000] for objects of solar metallicity: the minimum mass for a brown dwarf is about $13 M_J$ (where M_J is the mass of Jupiter) or $0.013 M_{sun}$, sufficient to allow deuterium burning; the minimum mass for a main sequence star is about $78 M_J$ or $0.075 M_{sun}$, sufficient to allow hydrogen burning.

Pulsar planets, known since 1992 from variations in pulse arrival times from pulsars, are kept in a separate category from exoplanets around main-sequence stars. These bodies may have formed during the explosion that created the neutron-star pulsar.

At least two websites collect current information on exoplanets. One site is "The Search for Extrasolar Planets" [*Marcy, 2001*] originating at UC Berkeley. The other, larger, site is "The Extrasolar Planets Encyclopaedia" [*Schneider, 2001*] originating at Paris Observatory, Meudon. Both sites feature news items, discussions, tutorials, papers, bibliographies, and comprehensive lists of exoplanets, their properties, and their parent stars. Both sites are expertly edited and authoritative.

The present paper is oriented toward extrasolar

terrestrial planets, i.e., those in the mass and temperature range of Venus, Earth, and Mars. However, since all known exoplanets are in the gas giant mass range, it is appropriate to ask about the prospects for finding terrestrial-mass exoplanets.

Astrometry (cf. later section) tells us the semi-major axis, eccentricity, and mass of a planet. Each of these is a clue to a part of the history of the planet, e.g., where and how it was formed, whether it has migrated since then, and whether its orbit has been perturbed by other bodies. However to learn from this data if terrestrial-sized planets might be present we must fall back on inference based on the observed frequency distribution of mass, as follows.

If we examine a plot of exoplanet mass versus semi-major axis, we see that the discoveries tend to populate the entire region between the extremes of: (a) maximum mass set by definition at about $13 M_J$; (b) minimum mass set by the radial velocity detection method at about $M/M_J = 0.035vR^{1/2}$ where v (m/s) is the minimum detectable orbital velocity amplitude and R (AU) is the orbital radius; (c) maximum radius set by a total observing time of about 5 years, to get a full orbit; and (d) minimum radius set by the smallest observed orbit at about 0.01 AU. If we assume that this entire region, on a $(\log R, \log M)$ plot, might be uniformly populated, then we can calculate the expected number of planets as a function of mass.

We show in Figure 1 a histogram of the detected masses, and two “expected” distributions corresponding to velocity amplitudes of 2 and 20 m/s, the former being a nominal goal of the present radial velocity searches, and the latter being an estimate of the current level of confident detection. Although Figure 1 is undoubtedly overly simple, we may nevertheless draw two conclusions. (1) At the high-mass end, where the present searches are certainly relatively complete and unbiased, the observed distribution drops off rapidly from about $1 M_J$ to $13 M_J$, suggesting that the exoplanet population really does exist as a separate entity from any brown dwarf population (not shown) which might fill in the $13\text{--}75 M_J$ range. (2) At the low-mass end, the observed population seems to be approximately fit by the 20 m/s curve, suggesting that the observations are observationally limited, and that there is no evidence for a fall-off at low masses. Thus at present we may well be sampling only the very top end of the exoplanet mass distribution curve, and it may well be that the distribution function continues all the way down to the M_{Earth} range. On this basis we optimistically look forward to someday finding

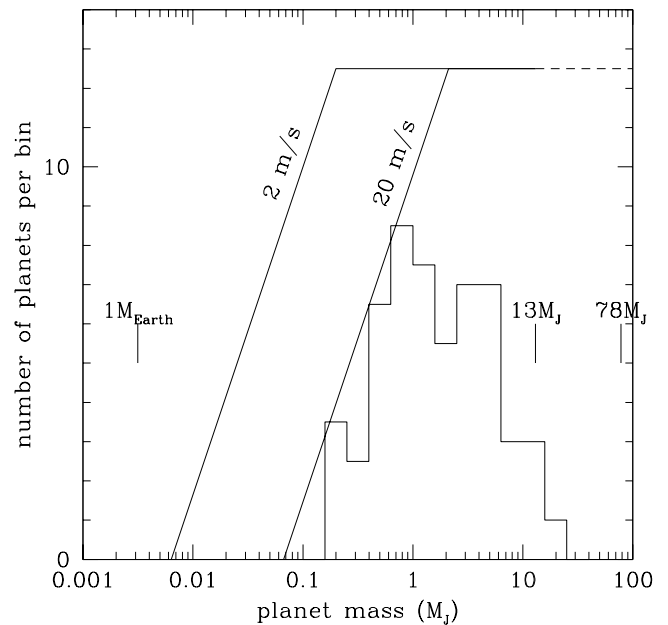


Figure 1. Histogram of discovered exoplanets, ranging from about 0.16 to $13 M_J$. Theoretical curves are shown for the cases where exoplanets have a uniform density distribution in the $(\log M, \log R)$ plane, in the range $\log M = -3$ to $+1.11$, and $\log R = -2$ to $+1$, and limited by the sensitivity of radial velocity measurements to orbital velocities of 2 and 20 m/s, as indicated. The observed distribution appears to be bounded by measurement accuracy on the low-mass side, and by a lack of exoplanets on the high-mass side.

terrestrial exoplanets.

2. DETECTION METHODS: GRAVITY AND AERONOMY

There is a surprising number of proposed techniques to detect or characterize exoplanets. About one-half of the techniques may be classified as being gravitational in nature, and the other half as being aeronomic (or photonic). The gravitational methods are (1) radial velocity, (2) astrometry, (3) transits, (4) pulsar timing, (5) gravitational lensing, and (6) disk shaping. The aeronomic methods are (7) visible-infrared shift, (8) reflected light, (9) transmitted light, (10) auroral emission, (11) radio emission, (12) anthropogenic transmission, (13) coronagraphic imaging, and (14) interferometric imaging.

2.1. Radial velocity

As the planet and star orbit their common center of mass, the velocity vector of the star projected along the observer's line of sight is proportional to $M \sin i$ where M is the planet mass and i is the inclination of the orbit plane to that of the sky. Doppler shifts in stellar spectra have been measured to an accuracy of about 3 m/s; 10 m/s is common, and 1 m/s may be the ultimate limit of this technique [Marcy and Butler, 2000; Santos *et al.*, 2000]. By comparison, the solar velocity due to Jupiter is about 3 m/s, and that due to Earth is about 0.01 m/s.

2.2. Astrometry

The projection of stellar orbital motion onto the plane of the sky produces an astrometric shift which is measured with respect to a grid of nearby reference stars. At 10 pc, Jupiter would move the Sun by about 100 μas (1 $\mu\text{as} = 10^{-6}$ arc-sec), and Earth would move the Sun by about 0.3 μas . The Hipparcos satellite had an accuracy of about 500 μas , so could not quite detect Jupiter-sized planets, but planned missions such as FAME (50 μas) [Horner *et al.*, 2001] (2004 launch planned), GAIA (2-10 μas) [Perryman *et al.*, 2001], (2012 launch planned), and SIM (1 μas) [Danner and Unwin, 1999] (2009 launch planned), have a good chance of detecting masses in the sub-Jupiter range, and almost down to the terrestrial limit.

2.3. Transits

If the planet's orbital plane is seen nearly edge-on, a partial eclipse of the star by the planet may occur. For the one example known to date, HD209458, [Charbonneau *et al.*, 2000], precise photometry has allowed us to infer the stellar limb darkening, the planet radius, the orbital inclination, and therefore the planet's mass. Further observation may lead to a transmitted light measurement, as discussed below. Dedicated, staring telescopic searches [*e.g.*, Borucki *et al.*, 2001] may detect more examples of this rare transit phenomenon.

2.4. Pulsar Timing

The clock-like constancy of pulsar spin rates means that the time delay produced by line of sight displacement due to an orbital companion can be interpreted in terms of the mass and orbit of the companion [*e.g.*, Konacki *et al.*, 2000]. Two such pulsars are known, PSR 1257+12 (3 planets, possibly 4),

and PSR B1620-26 (1 planet). Interestingly the technique is sufficiently sensitive that we know that some of these pulsar planets are in the few M_{Earth} range, and one may be in the M_{Pluto} range.

2.5. Gravitational Lensing

A star in our Galaxy can cause a distant light source (a background galaxy) to apparently brighten for several days by gravitationally deflecting and lensing the distant galaxy's light as the star happens to pass in front of the galaxy. If the star hosts a planetary companion, then the planet can cause a secondary brightening [Gaudi and Gould, 1997]. The effect would be transient, but statistics of many events would give information on the Galactic incidence of planets.

2.6. Disk Shaping

For a star with a debris disk, the presence of a planet with non-zero eccentricity or relative orbit inclination will cause the disk to become eccentric or warped, respectively; a planet inside the dust or debris disk can also generate resonant trapping (clumps) and clearing of central holes [Wyatt *et al.*, 1999; Liou and Zook, 1999].

2.7. Visible-Infrared Shift

Precise astrometry of an unresolved star-planet system in the visible and infrared wavelength regions simultaneously would show a spatial shift because the star light dominates the planet's light less in the infrared. This is a detection mode planned for the Keck Interferometer and Very Large Telescope Interferometer [Akeson *et al.*, 2000; Lopez *et al.*, 2000].

2.8. Reflected Light

For a large, close-in planet, sufficient star light may be reflected from the planet that it could be directly detected as an additional component of star light, even if the system is not spatially resolved [Charbonneau *et al.*, 1999].

2.9. Transmitted Light

If a planet eclipses the parent star, then the planet's transparent upper atmosphere will transmit a portion of the starlight, with a superposed planetary absorption spectrum which could produce measurable features such as He 1.0830 μm or Na 0.589 μm [Brown *et al.*, 2001].

2.10. Auroral Emission

Auroral activity such as seen on Earth or Jupiter (e.g., O 0.5577 μm , H α) is a non-thermal, potentially useful indicator of a planet [e.g., Waite *et al.*, 2001], but the flux rate may be so low as to not be competitive with other techniques. Detection of oxygen emission is discussed more fully in Chapter VI.2.

2.11. Radio Emission

Decametric radio wavelength radiation from electrons in the magnetic field around Jupiter and Io suggests that planets might be identified by this non-thermal radio signature [Bastian *et al.*, 2000], but low flux might limit this method.

2.12. Anthropogenic Transmissions

(a) It has been pointed out that a directed visible laser beam from Earth could be made to outshine the sun for the duration of a pulse, and would therefore be easily visible with a modest telescope at interstellar distances [Howard and Horowitz, 2001]. In the hope of detecting such pulses trial experiments have been started. (b) Pulsed radio transmissions containing coded messages are likewise detectable at great distance, and have been the basis of several searches [e.g., Horowitz and Sagan, 1993; Leigh and Horowitz, 1999].

2.13. Coronagraphic Imaging

Direct visible-wavelength detection of the analog of the solar system's gas giant outer planets could be achieved using existing general-purpose telescopes, such as the Hubble Space Telescope or the planned Next Generation Space Telescope, if the residual optical imperfections in either telescope were to be corrected by adaptive optics. Dedicated coronagraphic telescopes with shaped or shaded pupils have also been proposed [Nisenson and Papaliolios, 2001; Spergel, 2001]. To detect an Earth at 10 pc and 0.5 μm wavelength requires 10^{-10} starlight rejection at 0.1 arcsec separation.

2.14. Interferometric Imaging

An infrared-wavelength imaging interferometer has been proposed as a NASA mission [Beichman *et al.*, 1999], or European Darwin mission [Fridlund, 2000]. To detect an Earth at 10 pc and 10 μm wavelength requires 10^{-7} starlight rejection at 0.1 arcsec separation.

3. WHY SPECTRA OF TERRESTRIAL PLANETS?

Of all the techniques mentioned to detect or characterize an extrasolar terrestrial planet, we have chosen to focus on just two: coronagraphic imaging and interferometric imaging. The reason for this is that these seem to give us the best chance to determine the atmospheric constituents of the planet, by direct observation of the reflected or emitted light from the atmosphere and surface.

The current thumbnail picture of planetary formation is as follows. A massive molecular cloud is somehow triggered to collapse; a star is formed; the star is surrounded by a remnant gas and dust cloud; rocky, metallic, and, in the outer, colder parts of the cloud, icy grains, condense and agglomerate in the surrounding cloud; and the agglomerations cascade to larger sizes to form planetary cores. Then in the outer part of the cloud, where plenty of gas is available, the gas continues to collapse around the cores, and Jupiter-like (gas giant) planets form. In the inner part of the cloud where it is hotter and less gas is available, only rocky planets form. These rocky, terrestrial-type planets can have abundant liquid water or ice, and relatively thin atmospheric envelopes, both generated by outgassing of the rocky material and possibly also by infalling comets. It is on these planets, with their solid surfaces where water can accumulate and chemical reactions occur, and their thin atmospheres where sunlight can penetrate and be used for driving chemical reactions, that we speculate that life probably has its best chance to develop. (Excellent references can be found in Chyba *et al.* [2000], Lunine [1999], and Yung and DeMore [1999]).

Once we know the abundances of key gases, we can then make informed speculations on the likelihood that life exists on the planet. However even with the restriction to terrestrial-type planets, we still have a large range of possible types of atmospheres. In the following sections, we begin to explore the range of possibilities. We start with a description of our method for calculating visible and infrared spectra for the case of the present Earth. We extend this to include Neoproterozoic icehouse and hothouse Earths, a methane-rich Earth, and the present Mars and Venus. We conclude with a brief discussion of how the presence of life might be inferred from spectra such as these.

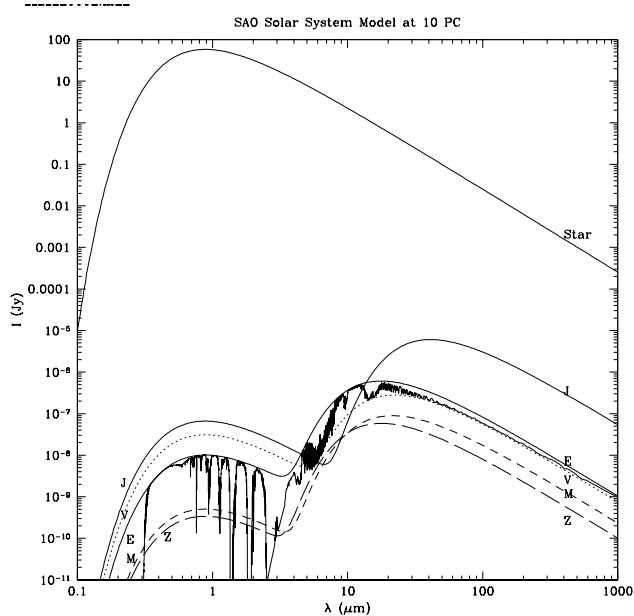


Figure 2. Solar system blackbody thermal emission spectra and reflected light spectra at 10 pc, for the Sun, Jupiter (J), Earth (E), Venus (V), Mars (M), and zodiacal dust (Z). For curve Z a telescopic field of view of 0.010 arcsec diameter centered at 0.1 arcsec from the star is assumed. For the Earth, present atmospheric abundances are used to calculate a line by line spectrum for the entire 4 decades in wavelength, for a cloud-free atmosphere. (Note 1 Jansky is 10^{-26} watt m^{-2} Hz^{-1} .)

4. PLANETARY SPECTRA: PRESENT EARTH

A graphical overview of the exoplanet detection issue is shown in Figure 2, where we plot the flux density of a model solar system as it would be seen from a distance of 10 pc, the median distance for the nearest 450 or so stars in our Galaxy.

Blackbody spectra of the Sun, Jupiter, and the 3 terrestrial planets are shown in Figure 2, for the effective temperatures of these bodies, except as follows: the spectrum of Jupiter includes its internal heat source contribution; the spectrum of Mars is an average of the day and night side spectra at different temperatures; and for Earth the average ground temperature is used, not the effective temperature. (N.B., the effective temperature of an object is the temperature of a blackbody which has the same area and total radiated power as does the object.)

The zodiacal dust cloud is modeled as a face-on, smooth, optically thin blackbody emitter with optical depth varying as $r^{-0.39}$ and temperature varying as $r^{-0.42}$ where r is distance from the central star [Reach, 1995].

The reflected light from Jupiter and the terrestrial planets is approximated by a scaled version of the solar spectrum, proportional to each planet's average visual albedo and area, reduced by a factor of 0.26 to approximate the brightness at quadrature, when the observer sees only one-half of the disk illuminated. The zodiacal dust reflection spectrum is modeled with the same density distribution as for the thermal emission but with an albedo selected to agree with visual observations.

The spectral line component of the Earth's spectrum in Figure 2 is calculated separately for the thermal emission and reflection cases, for a clear atmosphere, and the results combined, as described next.

4.1. Spectral Computation Method

Model Earth spectra are calculated with our SAO code originally developed to analyze balloon-borne far-infrared thermal emission spectra of the stratosphere [e.g., Traub and Stier, 1976; Johnson et al., 1995], extended to include visible reflection spectra. The spectral line data base includes the large AFGL compilation [Rothman et al., 1998] plus improvements from pre-release AFGL material and our own sources. In a few cases laboratory cross section spectra are available but spectroscopic analysis is not, so here we use an empirical pseudo-line band shape. The far wings of pressure-broadened lines can be non-Lorentzian at around 1000 times the line width and beyond, so in some cases (H_2O , CO_2 , N_2) we replace the far wings of the line-by-line calculation with measured continua data in these regions. Dust and Rayleigh scattering are approximated by empirical wavelength power laws and contribute significantly only in the visible blue range. Model atmospheres from 0 to 100 km altitude are constructed from standard models discretised to appropriate layers, and additional radiative transfer methods used to ensure that line cores and optically thick layers are accurately represented.

Radiative transfer from layer to layer is explicitly calculated using the average absorption and emission properties of each layer; scattering as a source is neglected. Integration from the spherical Earth atmosphere is approximated to a few percent accuracy by a single-point calculation at a zenith angle of 60 de-

grees, so the effective air mass is 2 in the infrared (outgoing emission) and 4 in the visible (2 for incoming sunlight, plus 2 for outgoing reflected light).

Cloud effects are beyond the scope of this chapter, and they are not included in the calculations shown here, but they can be represented by inserting continuum absorbing/emitting layers at appropriate altitudes; broken clouds can also be represented by a weighted sum of spectra using different cloud layers. In general, the effect of clouds is to dilute the strength of line features in the visible, and to dilute, but in extreme cases cause absorption lines to appear as emission lines, in the infrared.

4.2. Thermal Emission Spectrum

The dominant features of the Earth's thermal emission spectrum are illustrated in Figure 3, where the blackbody flux and composite spectrum (Jy/sr) are shown in the top left panel, and the other panels show the relative intensities of the major infrared molecular species (H_2O , O_3 , CH_4 , CO_2 , N_2O) as well as minor contributors (H_2S , SO_2 , NH_3 , SF_6 , CFC-11, CFC-12). The composite spectrum is calculated for the present abundances of each species, but the individual species spectra are calculated for increased or decreased abundances, with the expected vertical mixing ratio profiles scaled so as to show the absorption spectrum minima at an optical depth of about unity.

The H_2O panel shows the far-infrared rotational band and the mid-infrared vibrational band, calculated for an abundance of about 0.1 times the saturated value in the lower troposphere. Even at this reduced concentration, the water lines are quite strong, but also rather diffuse, without any well-defined compact spectral features in the thermal infrared.

Carbon dioxide, on the other hand, even at 5% of present abundance, shows a very strong $15\ \mu\text{m}$ ($667\ \text{cm}^{-1}$) band in the infrared, the depth of which is limited not by abundance, but rather by the thermal structure of the Earth's atmosphere, such that the minimum brightness corresponds to the blackbody strength at the altitude at which the band core optical depth reaches values on the order of unity. Note the small spike in the center which is generated at an altitude of about 30 km by the temperature inversion in the stratosphere, causing the very strong core to appear in emission against the lower-lying cooler layers from which the near-wing emission emanates at an altitude of about 20 km.

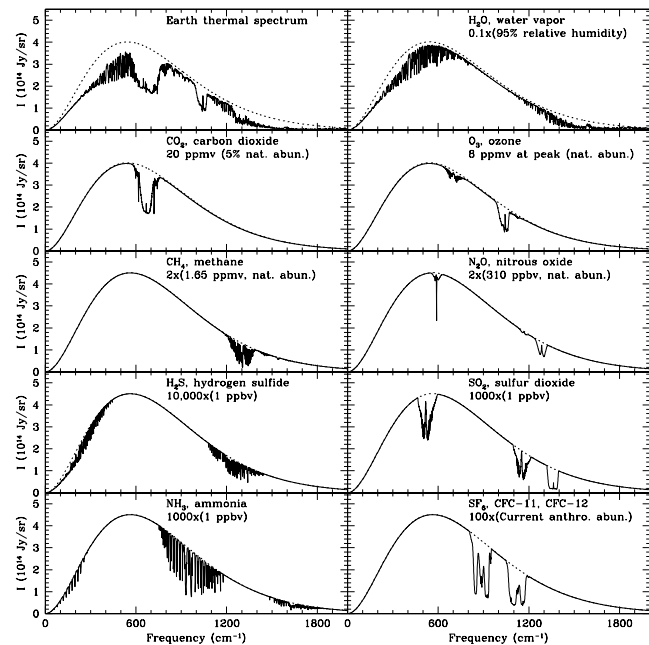


Figure 3. A calculated thermal emission spectrum of the present Earth is shown in the top left panel. The other panels show spectra of individual species, with their mixing ratio profiles scaled up or down so as to generate a maximum feature depth of roughly one-half. The calculations are performed at very high resolution and subsequently smoothed to $1\ \text{cm}^{-1}$ for display. The panels demonstrate the concentrations needed for each species to contribute significant opacities on an Earth-like planet.

Ozone is the third most prominent infrared feature with its strong $9\ \mu\text{m}$ ($1100\ \text{cm}^{-1}$) band, shown here at its natural abundance. The ozone feature is almost entirely due to the stratospheric O_3 layer, though there is a trace of tropospheric O_3 .

Methane and nitrous oxide are both shown at twice natural abundance, and have significant features nearly overlapping in the $7\ \mu\text{m}$ ($1400\ \text{cm}^{-1}$) region, also lying in the red wing of the $6\ \mu\text{m}$ ($1600\ \text{cm}^{-1}$) water band, and therefore not readily separable, but nevertheless in principle measurable. The combined effect of the current abundance of CH_4 and N_2O is seen in the composite panel, where the spectrum shows a rather sharp decrease going from about 1200 to $1300\ \text{cm}^{-1}$, compared to the gradual decrease in this region due to H_2O alone, as shown in the

water-only panel.

The remaining species, at present Earth abundances, are not expected to be easily detectable on an exoplanet, due to the weakness of their bands. The panels show H₂S at 10,000 times natural abundance, SO₂ at 1000 times, NH₃ at 1000 times, and the anthropogenic gases SF₆, CFC-11, and CFC-12 each at 100 times current abundance.

4.3. Reflection Spectrum

Dominant features in the present Earth's reflection spectrum are shown in Figure 4, where in this case the panels give the reflected intensity normalized to the incident solar intensity, smoothed from the original high-resolution calculation to a plotted resolution of 100. The upper left panel is a composite of the 5 contributing species H₂O, O₂, O₃, CH₄, and CO₂, for present abundances. Note that the spectral range goes from the near infrared (2000 cm⁻¹ = 5 μm) to the near ultraviolet (33000 cm⁻¹ = 0.30 μm), with a continuum normalized everywhere to unity. We have ignored the thermal emission contribution at long wavelengths as well as the Rayleigh and dust scattering components which will show up mostly at short wavelengths.

The H₂O panel, for the present abundance of water, shows a series of absorption bands spanning the middle part of the visible spectrum and increasing in strength toward the near infrared. The strengths of these vibrational bands are essentially independent of temperature, but will increase in proportion to the abundance of water and the square root of air pressure, however since the lines are relatively saturated, the average band depth will only increase as the square root of band strength. The net result is that these bands should be good indicators of the presence of water over a large dynamic range of conditions, although this same property makes them less useful as quantitative indicators of water mixing ratio, unless we also have independent knowledge of temperature and pressure.

The strongest O₂ band is the Fraunhofer A-band at 0.76 μm (13000 cm⁻¹). This band too is saturated, and will still be relatively strong for significantly smaller mixing ratios than the present Earth's. It will therefore be an excellent indicator of the presence of oxygen (see Chapter VI.2).

The O₃ molecule has two broad features of note, the extremely strong Huggins band which produces the ultraviolet absorption shown here at about 0.33

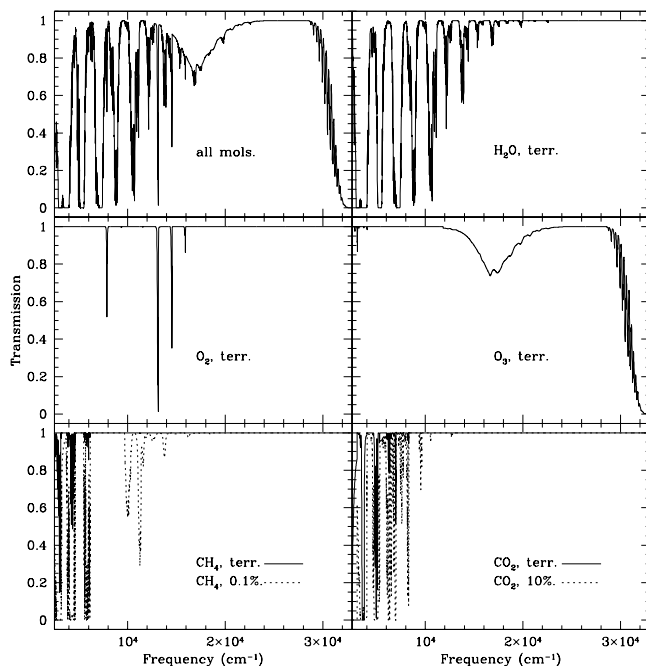


Figure 4. The reflectivity of the Earth with present atmospheric abundances is shown in the top left panel, normalized to unity. Clouds, aerosols, and Rayleigh scattering are ignored in this example. The other panels show reflection spectra for the cases where only a single species is present in terrestrial abundances. For CH₄ and CO₂ we also show spectra for greatly enhanced abundances as discussed in the text.

μm (30000 cm⁻¹) and shorter, and the Chappuis band which shows up as a broad triangular dip in the middle of the visible spectrum from about 0.45 to 0.74 μm (22000–13000 cm⁻¹). Ozone in the stratosphere is produced from O₂ molecules, and its abundance is a non-linear function of the O₂ abundance, such that even a small amount of O₂ can produce a relatively large amount of O₃ [Kasting and Donahue, 1980]; however in absolute terms the modeled column abundance of O₂ is nevertheless large compared to that of O₃ by a factor of 20,000 to 500,000.

Methane at present terrestrial abundance (1.65 ppmv) has no significant visible absorption features, but at high abundance (0.1%) it has strong visible bands at 0.9 and 1.0 μm (11000 and 10000 cm⁻¹).

Carbon dioxide has negligible visible features at present abundance, but in a high-CO₂ atmosphere (10%) it has a significant band at 1.2 μm (8000 cm⁻¹)

and even stronger ones at longer wavelengths.

5. PLANETARY SPECTRA: NEOPROTEROZOIC EARTH

The present status of our secure knowledge of paleo-Earth atmospheres is easy to review, because little of our knowledge is secure, although in recent years the situation has been improving. In overview, the evolution of CO₂ has long been believed to have decreased from a high level of roughly 1 bar at about 4.5 Ga (where Ga represents 1×10^9 years ago) to 0.00035 bar at present, however recent evidence suggests that major oscillations occurred around 0.5–0.8 Ga, and perhaps at other glaciations. The abundance of O₂ is believed to have been less than 0.001 bar until about 2 Ga when it rapidly began to increase toward its 0.2 bar present value, and the time of transition is roughly coincident with the beginning of abundant phytoplankton on Earth.

The equilibrium temperature of the Earth with its present albedo, present solar flux, and no greenhouse gases is about 246 K, below the freezing point of water; this corresponds to the physical temperature at a level in the stratosphere at which the Earth effectively radiates. The Earth is rescued from freezing by the greenhouse effect, which can be envisioned as being driven at temperatures below the freezing point of water by CO₂ and aided at higher temperatures by evaporated water vapor. The combination of present levels of CO₂ and H₂O is sufficient to warm the surface to 290 K, about the current average surface temperature, which is of course sufficient for liquid water.

The early Earth was illuminated by a weaker Sun, about 0.71 times the present luminosity, which without CO₂ would have resulted in an even cooler Earth, about $246(0.71)^{1/4} = 226$ K. The argument for a large amount of early CO₂ is simply that we believe that liquid water, with only intermittent glaciation, was present during most of Earth's past [*cf. e.g., Lunine* 1999, Sec. 11.10 and 19.4], and this requires a large greenhouse effect, equivalent to about 0.2 bar or more CO₂. Also, since there is the equivalent of about 50 bar of CO₂ deposited in crustal rocks, the pressure may have been higher.

The level of CO₂ probably did not fall steadily since 4.5 Ga. We know that periods of major glaciation did occur, and that almost certainly these could not have begun unless the CO₂ abundance had first dropped significantly. Recently there has been a major advance in this area with the clear-cut identifi-

cation of 3 major glaciation cycles alternating with warm tropical conditions at about 0.5–0.8 Ga [*Hoffman et al., 1998*]. This period is roughly the end of the Proterozoic era (from 4.5 to 0.7 Ga), and the start of the Phanerozoic era (from 0.7 to 0.0 Ga), so the sudden glaciations are said to have produced a Neoproterozoic “snowball” Earth. The CO₂ abundances probably oscillated between roughly 0.2 bar and 0.0001 bar. The evidence for oscillation is unambiguously seen in rock layers in Namibia: repeated pairings of rounded boulders (from glaciers) topped by thick layers of carbonate rock (precipitated from seawater).

A major mystery is why these oscillations have not occurred over most of Earth's history, or more pointedly, why the oscillations started when they did and stopped after a few cycles. It is possible that the other major glaciations were accompanied by such oscillations, but this has not yet been established, or even discussed, to our knowledge.

One might expect that the icehouse state would be triggered by a sudden drop in CO₂, caused perhaps by a rapid uptake of CO₂ in the ocean, for some reason, and that the hothouse state would be triggered by the accumulation of volcanic CO₂, a direct result of plate tectonics, which at present rates would take only a geologically short interval of about 10 million years to reach greenhouse levels. However the details of the oscillations are as yet not well understood.

The implication of the Neoproterozoic oscillations for extrasolar planet searching is clear: we might encounter such a condition on an extrasolar planet, and we must be prepared to anticipate its spectral signature. We show in Figure 5 our preliminary calculation of the infrared spectra of a Neoproterozoic hothouse and icehouse Earth. To simulate the icehouse state, we use the present Arctic temperature profile, and O₂ at 1% PAL (present atmospheric level); the O₃, H₂O, N₂O, and CH₄ are modified [*Kasting, 1980*] for a 1% O₂ level, and the CO₂ is set to 100 ppm; about 1 bar of N₂ is also assumed to be present. To simulate the hothouse state, we used a present tropical temperature profile, O₂ at 10% PAL, and corresponding O₃, H₂O, N₂O, and CH₄; also CO₂ is set to 120,000 ppm.

A substantial literature is building on the snowball Earth concept, for example climate simulations [*Jenkins and Smith, 1999; Hyde et al., 2000*] and realizations that life would not be totally eliminated by ice cover [*Runnegar, 2000*].

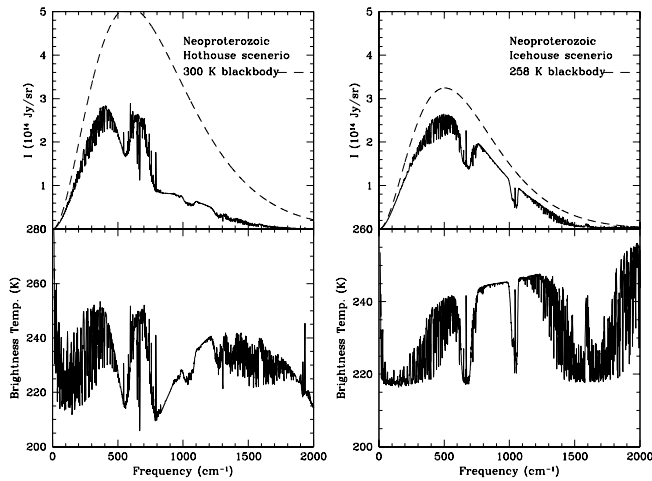


Figure 5. A calculated thermal infrared emission spectrum for a Neoproterozoic hothouse condition (left), and icehouse (right). Note the huge difference between these; for example, the $15\ \mu\text{m}$ CO_2 feature is an apparent emission feature in the hothouse spectrum, but it is an apparent absorption feature in the icehouse spectrum. The apparent emission feature is a result of a warm inversion layer in the stratosphere (due to O_3 heating) combined with a CO_2 mixing ratio which gives an optical depth of about unity at the top of this layer for wavelengths in the core of the CO_2 band.

6. PLANETARY SPECTRA: METHANE

Besides CO_2 , methane (CH_4) could strongly influence the surface temperature of a planet. Methane bursts may have punctuated the Earth’s history. For example, carbon and oxygen isotope fractionation in marine carbonate deposits strongly imply that about 350 times the present level of CH_4 was injected into the Earth’s atmosphere, during a span of less than 1000 years, about 0.055 Ga [Bains *et al.*, 1999]. The source of the CH_4 may well have been methane hydrate, which is found on the sea floor in abundance even today. That this time of injection coincided closely with a period of warming (the Late Paleocene thermal maximum) strongly suggests a cause and effect relationship between these phenomena, but it is not clear which is cause and which is effect.

Further evidence for a methane burst has been

found at another epoch, 0.183 Ga [Hesselbo *et al.*, 2000]. This event is associated with high surface temperatures and significant mass extinction. Yet other such events at 0.090 and 0.120 Ga have been similarly reported [Kerr, 2000]. Interestingly, each of these events, now 5 in total, occurs at about the same time that a large volume of volcanic outflow occurred, and a corresponding mass extinction occurred, suggesting that perhaps the volcanoes triggered the methane and this in turn triggered further warming which resulted in large-scale loss of species. Large amounts of CH_4 , such as in these bursts, will produce measurable absorption features in both the infrared emission and near-infrared absorption spectra of the Earth.

7. PLANETARY SPECTRA: PRESENT VENUS AND MARS

We have calculated infrared spectra of Venus and Mars, using current models of atmospheric abundances and temperature profiles, with the added factor that the opacities of air-borne dust and aerosol droplets can be included in order to reproduce observed silicate and ice features. Clearly we have much less information on the geologic history of these planets than we do for Earth, but spectral evidence of isotopic fractionation on both planets has led to informed speculation about the past abundance of water, for example.

We show in the right panel of Figure 6 our calculated Mars spectrum using a recent model atmosphere [Y. Yung, 1999, private communication]. The CO_2 and H_2O features in this spectrum are a good match to many observed Mars spectra. We have repeated these calculations with the inclusion of thin ice clouds and silicate dust clouds, and these provide a reasonably good simulation of certain other observed Mars spectra. The calculations for Venus are shown in the left panel of Figure 6, based on the model atmosphere of Bullock and Grinspoon [2001]. This spectrum is dominated by CO_2 , and does not include any aerosols, so the fact that the very bright thermal emission from the ground is not seen at the top of the atmosphere is entirely due to the opacity of the wings of the strong CO_2 bands.

8. CAN WE DETECT LIFE?

The big question, can we detect life on an extrasolar planet, was addressed in a general sense by Lovelock, [1965] who advocated searching for signs of

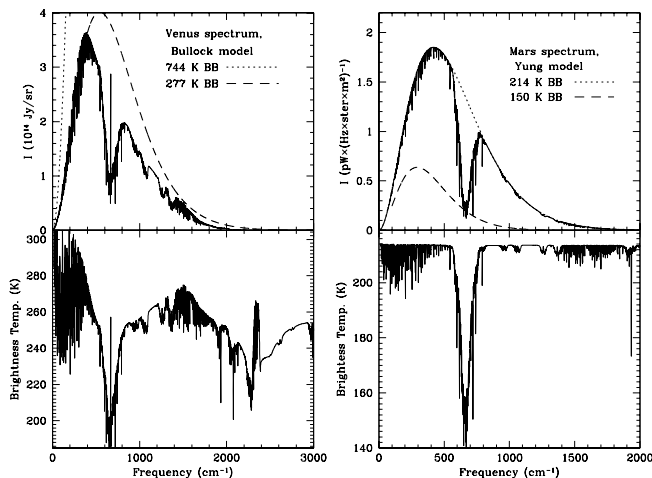


Figure 6. Calculated spectra for Venus and Mars. Both spectra are dominated by CO_2 . No ice or dust features are included here, although these features are seen occasionally on Mars, and we have modeled them successfully.

chemical non-equilibrium, such as the simultaneous presence of reducing and oxidizing gases. In principle, if one knew the abundances of all species present in an atmosphere, and the boundary conditions (incident spectrum from star, surface composition, rotation rate, etc.), then one could calculate the state of photochemical and dynamical equilibrium, and its likely fluctuations, and compare this with the observed state, to see if there are significant differences which might be interpreted as signs of life, a term not included in the equilibrium calculation [*cf. Nisbet and Sleep, 2001; Brack, 1998*]. However our experience with the atmosphere of the present Earth tells us that the observed state is frequently not predicted by theory, so this approach may not be foolproof

From a spectroscopic point of view, it is natural to think of searching for life in terms of measuring the abundances of atmospheric constituents, and comparing these abundances with the results of calculations of thermochemical and photochemical equilibrium. In particular, the simultaneous presence of significant amounts of oxidized and reduced species, such as H_2O , CO_2 , N_2O , and CH_4 , or the presence of large amounts of O_2 or O_3 , would both be indicators of life. Indeed both conditions are found on Earth, where there is no known means of producing

anything approaching a 21% O_2 atmosphere except by photosynthesis, and the main sources of N_2O and CH_4 are biological. Earth's O_3 is produced in relatively large amounts in the stratosphere by photolysis and recombination of O_2 , making it a good indicator of the presence of O_2 . As signs of life in themselves, H_2O and CO_2 are secondary in importance, because although they are raw materials for life, they are not unambiguous indicators of its presence. Farther down the chain, CH_4 is a life product on Earth, but elsewhere it is also a ubiquitous primordial species, and it is difficult to detect spectroscopically unless it is quite abundant. Likewise, N_2O is interesting because it is produced in abundance by life, and only in trace amounts by natural processes, but it can only be detected in a region which is strongly overlapped by CH_4 and H_2O , and so is an unlikely prime target.

As counterexamples, we know that small amounts of O_2 and O_3 are readily produced by non-biological means. For example, a trace amount of O_2 is seen on Venus, consistent with photochemical production from CO_2 ; on Mars both O_2 and O_3 are measured, but the amounts are in agreement with calculations of photochemical production from CO_2 and loss due to CO_2 and H_2O and products [*e.g., Yung and DeMore, 1999*]. In two other examples, Europa has about 10^{-11} bar of O_2 in its atmosphere (e.g., Chapter III.3), and Ganymede may have O_2 trapped in surface ice, but in both cases the observed signatures are consistent with energetic particle bombardment of a water-ice surface, and therefore they do not require a biological source.

An intriguing theory of the origin of life on Earth [*Wächtershäuser, 2000*] has found experimental backing in new laboratory experiments [*Cody et al., 2000*] which show that iron sulfide at elevated pressure and temperature can facilitate the natural generation of organometallic compounds by an autocatalytic process, in which the products of reaction catalyze the next cycle of reaction, making the process likely to be self-sustaining. This work is of interest because iron and sulfur atoms are at the center of many enzymes, and the process provides a simple explanation of their presence in living cells. The work is also of interest because it suggests that the origin of life on Earth may have been deep underground, where conditions are right for the reactions to take place, and out of the possibly less-friendly conditions on the surface of the early Earth.

The Neoproterozoic oscillations discussed above may also be critically important to the development

of life on Earth, because, as the eponymic oscillations suggest, this era coincided with the explosive radiation of life forms on Earth, from simple algae types to the dramatically different types of life forms we know today. It is thought that the huge stresses, due to oscillations of temperature, nutrients, and available sunlight, imposed on simple life forms forced them to develop new adaptations in order to survive in their new environments, in what may have been the greatest Darwinian experiment ever. Thus, if we find extrasolar planets in the throes of such oscillations, we may expect that a similar life-radiation may be occurring on that planet, although we will have to wait another several tens or hundreds of million years before we can see how the experiment turns out.

Acknowledgments. This work at SAO was supported by NASA via contract JPL 1201749, and via the TPF program through a contract to Ball Aerospace & Technologies Corp.

References

- Akeson, R.L., M.R. Swain, and M.M. Colavita, Differential phase technique with the Keck Interferometer, *SPIE*, 4006, pp. 321–327, 2000.
- Bains, S., R.M. Corfield, and R.D. Norris, Mechanisms of climate warming at the end of the Paleocene, *Science*, 285, p. 724–727, 1999.
- Bastian, T.S., G.A. Dulk, Y. Leblanc, A search for radio emission from extrasolar planets, *Ap.J.*, 545, pp. 1058–1063, 2000.
- Beichman, C.A., N.J. Woolf, and C.A. Lindensmith, editors, The Terrestrial Planet Finder (TPF): A NASA Origins program to search for habitable planets, JPL Publication 99-3, 158 pp., 1999. Also see <http://tpf.jpl.nasa.gov/>.
- Borucki, W.J. D.A. Caldwell, D.G. Koch, L.D. Webster, J.M. Jenkins, Z. Ninkiv, and R. Showen, The Vulcan photometer: a dedicated photometer for extrasolar planet searches, *PASP*, 113, pp. 439–451, 2001.
- Brack, A., editor, The Molecular Origins of Life, 417 pp., Cambridge University Press, New York, 1998.
- Brown, T.M., et al., Transmission spectra as diagnostics of extrasolar giant planet atmospheres *Ap.J.*, 553, pp. 1006–1026, 2001.
- Bullock, M.A., and D.H. Grinspoon, The recent evolution of climate on Venus, *Icarus*, 150, pp. 19–37, 2001.
- Charbonneau, D., R.W. Noyes, S.G. Korzennik, P. Nissen, S. Jha, S.S. Vogt, and R.I. Kibrick, An upper limit on the reflected light from the planet orbiting the star tau Bootis, *Ap.J.Lett.*, 522, pp. L145–L148, 1999.
- Charbonneau, D., T.M. Brown, D.W. Latham, and M. Mayor, Detection of planetary transits across a Sun-like star, *Ap.J.Lett.*, 529, pp. L45–L48, 2000.
- Chyba, C.F., D.P. Whitmire, and R. Reynolds, Planetary habitability and the origins of life, in *Protostars and Planets IV*, edited by V. Mannings, A.P. Boss, and S.S. Russell (Univ. of Arizona Press), pp. 1365–1393, 2000.
- Cody, G.D., N.Z. Boctor, T.R. Filley, R.M. Hazen, J.H. Scott, A. Sharma, and H.S. Yoder, Primordial carbonylated iron-sulfur compounds and the synthesis of pyruvate, *Science*, 289, pp. 1337–1340, 2000.
- Danner, R., and S. Unwin, editors, Space Interferometry Mission, JPL 400-811, 139 pp., 1999; also <http://sim.jpl.nasa.gov>.
- Fridlund, M., editor, Darwin, the infrared space interferometer, concept and feasibility study report, ESA Publication ESA-SCI(2000)12, 218 pp., 2000.
- Gaudi, B.S., and A. Gould, Planet parameters in microlensing events, *Ap.J.*, 486, pp. 85–99, 1997.
- Hesselbo, S.P., D.R. Groccke, H.C. Jenkyns, C.J. Bjerrum, P. Farrimond, H.S. Morgans Bell, and O.R. Green, Massive dissociation of gas hydrate during a Jurassic oceanic anoxic event, *Nature*, 406, p. 392–395, 2000.
- Hoffman, P.F., A.J. Kaufman, G.P. Halverson, and D.P. Schrag, A Neoproterozoic snowball Earth, *Science*, 281, pp. 1342–1346, 1998.
- Horner, et al., The full-sky astrometric mapping explorer - astrometry for the new millennium, in *Working on the Fringe*, edited by S.C. Unwin and R.V. Stachnik (ASP Conference Series) in press, 2001.
- Horowitz, P., and C. Sagan, Five years of project META - an all-sky narrow-band radio search for extraterrestrial signals, *Ap.J.*, 415, pp. 218–235, 1993.
- Howard, A., and P. Horowitz, Optical SETI with NASA's Terrestrial Planet Finder, *Icarus*, 150, pp. 163–167, 2001.
- Hyde, W.T., T.J. Crowley, S.K. Baum, and W.R. Peltier, Neoproterozoic 'snowball Earth' simulations with a coupled climate/ice-sheet model, *Nature*, 405, pp. 425–429, 2000.
- Jenkins, G.S., and S.R. Smith, GCM simulations of snowball Earth conditions during the late Proterozoic, *GRL*, 26, p. 2263–2266, 1999.
- Johnson, D.G., K.W. Jucks, W.A. Traub, and K.V. Chance, The Smithsonian stratospheric far-infrared spectrometer and data reduction system, *J. Geophys. Res.*, 100, pp. 3091–3106, 1995.
- Kasting, J.F., and T.M. Donahue, The evolution of atmospheric ozone, *JGR*, 85, pp. 3255–3263, 1980.
- Kerr, R.A., Did volcanoes drive ancient extinctions?, *Science*, 289, pp. 1130–1131, 2000.
- Konacki, M., A.J. Maciejewski, and A. Wolszczan, Improved timing formula for the PSR B1257+12 planetary system, *Ap.J.*, 544, pp.921–926, 2000.
- Leigh, D., and P. Horowitz, Strategies, Implementation and Results of BETA, Bioastronomy 99: a new era in bioastronomy. 6th bioastronomy meeting, Kohala Coast Hawaii, August 2-6, 1999.
- Liou, J.-C., and H.A. Zook, Signatures of the giant plan-

- ets imprinted on the Edgeworth-Kuiper belt dust disk, *Astron. Journ.*, *118*, pp. 580–590, 1999.
- Lopez, B., R.G. Petrov, and M. Vannier, Direct detection of hot extrasolar planets with the VLTI using differential interferometry, *SPIE*, *4006*, pp. 407–411, 2000.
- Lovelock, J.E., A physical basis for life detection experiments, *Nature*, *207*, pp. 568–570, 1965.
- Lunine, J.I., Earth: evolution of a habitable world, 319 pp., Cambridge Univ. Press, New York, 1999.
- Marcy, G., and P.R. Butler, Planets orbiting other suns, *PASP*, *112*, pp. 137–140, 2000.
- Marcy, G., *The search for extrasolar planets*, at the web site <http://exoplanets.org>, 2001.
- Nisbet, E.G., and N.H. Sleep, The habitat and nature of early life, *Nature*, *409*, pp. 1083–1091, 2001.
- Nisenson, P., and C. Papaliolios, Detection of Earth-like planets using apodized telescopes, *Ap. J. Lett.*, *548*, pp. L201–L205, 2001.
- Oppenheimer, B.R., S.R. Kulkarni, and J.R. Stauffer, Brown dwarfs, in *Protostars and Planets IV*, edited by V. Mannings, A.P. Boss, and S.S. Russell (Univ. of Arizona Press), pp. 1313–1338, 2000.
- Perryman, M.A.C., K.S. de Boer, G. Gilmore, E. Hg, M.G. Lattanzi, L. Lindegren, X. Luri, F. Mignard, O. Pace, P.T. de Zeeuw, GAIA: composition, formation and evolution of the galaxy, *Astron. & Astrophys.*, *369*, pp. 339–363, 2001.
- Reach, W.T., Zodiacal emission. III. Dust near the asteroid belt, *Ap. J.*, *392*, pp. 289–299, 1992.
- Rothman, L.S., C.P. Rinsland, A. Goldman, S.T. Massie, D.P. Edwards, J.-M. Flaud, A. Perrin, C. Camy-Peyret, V. Dana, J.-Y. Mandin, J. Schroeder, A. McCann, R.R. Gamache, R.B. Wattson, K. Yoshino, K.V. Chance, K.W. Jucks, L.R. Brown, V. Nemtchinov, and P. Varanasi, The HITRAN molecular spectroscopy database and HAWKS (HITRAN atmospheric workstation): 1996 edition, *J.Q.S.R.T.*, *60*, pp. 665–710, 1998.
- Runnegar, B., Paleoclimate: loophole for snowball Earth, *Nature*, *405*, p.403, 2000.
- Santos, N.C.; M. Mayor, D. Naef, F. Pepe, D. Queloz, S. Udry, A. Blecha, The CORALIE survey for southern extra-solar planets. IV. Intrinsic stellar limitations to planet searches with radial-velocity techniques, *Astron. & Astrophys.*, *361*, pp. 265–272, 2000.
- Schneider, J., *The extrasolar planets encyclopaedia*, <http://cfa-www.harvard.edu/planets/>, (US mirror site for <http://www.obspm.fr/encycl/encycl>), 2001.
- Spergel, D.N., A new pupil for detecting extrasolar planets, *Appl. Optics*, submitted, 2001.
- Traub, W.A., and M.T. Stier, Theoretical atmospheric transmission in the mid- and far-infrared at four altitudes, *Appl. Opt.*, *15*, pp. 364–377, 1976.
- Wachtershauser, G. Life as we don't know it, *Science*, *289*, pp. 1307–1308, 2000, and references therein.
- Waite, J.H., G.R. Gladstone, W.S. Lewis, R. Goldstein, D.J. McComas, P. Riley, R.J. Walker, P. Robertson, S. Desai, J.T. Clarke, and D.T. Young, An auroral flare at Jupiter, *Nature*, *410*, pp. 787–789, 2001.
- Wyatt, M.C. S.F. Dermott, C.M. Telesco, R.S. Fisher, K. Grogan, E.K. Holmes, R.K. Pia, How observations of circumstellar disk asymmetries can reveal hidden planets: pericenter glow and its application to the HR 4796 disk, *Ap.J.*, *527*, pp. 918–944, 1999.
- Yung, Y.L., and W.B. DeMore, Photochemistry of planetary atmospheres, 455 pp., Oxford University Press, New York, 1999.
-
- W. A. Traub and K. W. Jucks, Harvard-Smithsonian Center for Astrophysics, 60 Garden Street, Cambridge, MA 02138.
(email: wtraub@cfa.harvard.edu, kjucks@cfa.harvard.edu)

This preprint was prepared with AGU's L^AT_EX macros v4. File paper020520 formatted November 9, 2018.

With the extension package 'AGU++', version 1.3 from 1995/12/01